Supplementary Information

Buffering internal thermal surges: the role of precursor specific heat capacity in the microstructural integrity of $LiNiO_2$ cathodes

Woowon Chung,[a,1] Young Geol Yu,[b,1] JinHa Shim,[b] and Jin Ho Bang [b,c,*]

[a] Department of Bionano Technology, Center for Bionano Intelligence Education and Research, Hanyang University ERICA, 55 Hanyangdaehak-ro, Sangnok-gu, Ansan, Gyeonggi-do 15588, Republic of Korea

[b] Department of Applied Chemistry, Center for Bionano Intelligence Education and Research, Hanyang University ERICA, 55 Hanyangdaehak-ro, Sangnok-gu, Ansan, Gyeonggi-do 15588, Republic of Korea

[c] Department of Energy and Bio Sciences, Hanyang University ERICA, 55 Hanyangdaehak-ro, Sangnok-gu, Ansan, Gyeonggi-do 15588, Republic of Korea

AUTHOR INFORMATION

[1] These authors contributed equally to this work.

Corresponding Author:

*jbang@hanyang.ac.kr

Experimental Section

1. *Synthesis of size-controlled $Ni(OH)_2$ precursors*

$Ni(OH)_2$ precursors with target particle sizes of 4 μm, 8 μm, and 12 μm were synthesized via a co-precipitation method. Aqueous solutions of 2 M $NiSO_4 \cdot 6H_2O$ (98.5%, Samchun) as the metal source, 3 M NH_4OH (Duksan) as the chelating agent, and 5 M NaOH (Duksan) as the pH controller were prepared. The synthesis was conducted in a 5 L reactor under a continuous high-purity N_2 atmosphere. The particle sizes of the precursors were systematically controlled by adjusting the agitation speed (800–1000 rpm), reaction time (24–48 h), and pH (10.5–11.1). To ensure a uniform particle size distribution and remove residual impurities, the resulting precipitates were thoroughly washed multiple times with distilled water and collected via vacuum filtration. Finally, the obtained precursor powders were dried in a vacuum oven at 80 °C for 12 h.

2. *Calcination of $LiNiO_2$*

The synthesized $Ni(OH)_2$ precursors were mixed with $LiOH \cdot H_2O$ at a molar ratio of 1:1.03. The mixture was initially ground in a mortar and subsequently homogenized using a planetary centrifugal mixer (AR-100, THINKY Corp.) for 10 min. Calcination was performed in a tube furnace (SH-FU-50STG-WG, SH Scientific) under an O_2 atmosphere with a flow rate of 0.6 L min^{-1}, regulated by a mass flow controller (MF-200CV, MFC Flow). The samples were heated at 500 °C for 5 h and subsequently at 650 °C for 10 h, employing a heating rate of 2 °C min^{-1}.

3. *Material characterization*

Particle morphology and size were examined using a scanning electron microscope (SEM, VEGA3, Tescan), and the particle size distribution of each sample was determined using ImageJ software. X-ray diffraction (XRD, MiniFlex600, Rigaku) with Cu K_α radiation was utilized to investigate the crystallinity and crystal structure of the synthesized LNO samples.

The XRD patterns were recorded in the 2θ range of 10° to 140° at a scan rate of 1° min^{-1}, and the data were refined by the Rietveld method using TOPAS software. The elemental compositions of Li and Ni were quantified by inductively coupled plasma atomic emission spectrometry (ICP-AES, Avio 200, PerkinElmer). Thermogravimetric analysis (TGA) and differential scanning calorimetry (DSC, SDT-Q600, TA Instruments) were conducted using a thermal analyzer (SDT-Q600, TA Instruments) at various heating rates (5, 10, 15, 20, and 25 °C min^{-1}) under an O_2 flow. The oxidation states of the transition metals were analyzed via X-ray photoelectron spectroscopy (XPS, PHI VersaProbe). The Brunauer–Emmett–Teller (BET) surface area was determined from the analysis of nitrogen (N_2) adsorption/desorption isotherms obtained by a BELSORP MINI II (BEL Japan) instrument.

4. *Measurement of specific heat capacity*

The specific heat capacity (C_p) of the $Ni(OH)_2$ precursors was determined using DSC via the standard sapphire method. To ensure high precision and correct for instrumental artifacts, such as baseline drift, a systematic three-step protocol was employed. First, a baseline was established using empty alumina pans to subtract the instrumental background. Second, a sapphire reference standard (12.238 mg), possessing a known C_p of 0.774 J g^{-1} K^{-1} at room temperature, was measured; the experimental accuracy was confirmed to be within a 2% error margin. Finally, the $Ni(OH)_2$ samples were analyzed under identical thermal profiles and mass loadings. The specific heat capacity was calculated using the instrument's dedicated analysis software.

5. *In situ XRD characterization*

In situ XRD measurements were performed using a PANalytical Empyrean diffractometer at 25 °C to monitor the crystal structure evolution of the electrodes during electrochemical cycling. Data were collected over a 2θ range of 10° to 80° at a scan rate of 1° min^{-1}. A custom-designed

electrochemical cell equipped with a beryllium window was employed to facilitate X-ray transmission, and the electrochemical cycling was conducted at a current rate of 0.1C.

6. *Electrochemical characterization*

The cathode slurry was prepared by mixing the active material, a conductive agent, and a binder in a weight ratio of 85:7.5:7.5 in *N*-methyl-2-pyrrolidone using a planetary mixer (AR-100). The slurry was coated onto an aluminum foil current collector using an Auto Mini Coater (MC Corp.) and dried in a vacuum oven at 100 °C for 12 h. The dried electrodes were subsequently calendered using a roll press. The mass loading of the active material was approximately 4.0 mg cm^{-2}. For the full-cell evaluations, the cathodes were prepared with areal loadings comparable to those used in the half-cell tests, and the anode-to-cathode capacity (N/P) ratio was controlled within the range of 1.1–1.2.

CR2032 coin-type cells (Sinopromrx) were assembled in an argon-filled glove box with H_2O and O_2 levels maintained below 1.0 ppm. Lithium metal was used as the counter electrode for the half-cells, and a Celgard 2400 microporous membrane served as the separator. The electrolyte for the half-cells consisted of 1.13 M $LiPF_6$ dissolved in a solvent mixture of ethylene carbonate, dimethyl carbonate, and ethyl methyl carbonate in a 3:4:3 volume ratio. For the full-cell evaluations, the electrolyte consisted of 1.2 M $LiPF_6$ in a 3:7 (v/v) mixture of ethylene carbonate and ethyl methyl carbonate, with 5 wt% vinylene carbonate as an additive. Galvanostatic charge-discharge tests were performed using a battery cycler (WBCS3000, WonAtech) at 25 °C. Half-cells were evaluated in the voltage range of 2.7–4.3 V (vs. Li^+/Li) after an initial formation cycle at 0.1C. Subsequent long-term cycling was performed at a rate of 0.5C, and at various rates for rate capability tests (1C = 200 mA g^{-1}). Full-cells were evaluated in the voltage range of 2.5–4.2 V. Similar to the half-cells, an initial formation cycle was conducted at 0.1C, followed by long-term stability testing at a rate of 0.5C.

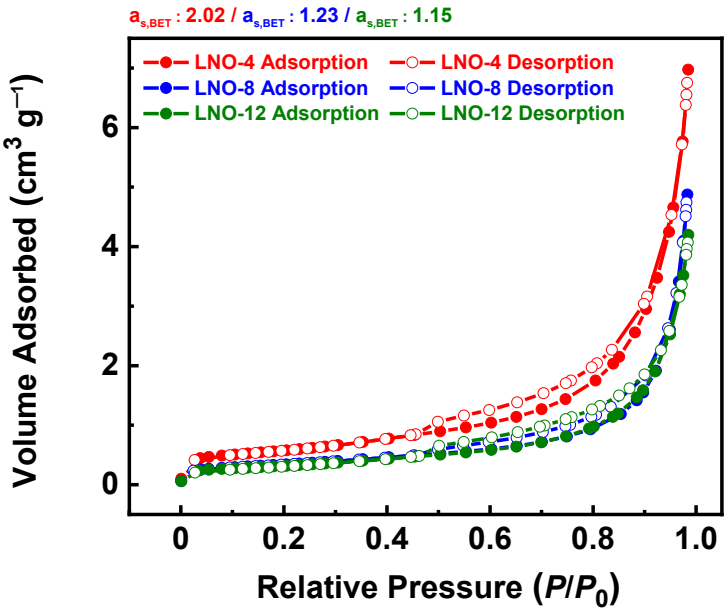

Fig. S1 N_2 adsorption–desorption isotherms of the $Ni(OH)_2$ precursors corresponding to LNO-4, LNO-8, and LNO-12. The BET specific surface areas of the LNO-4, LNO-8, and LNO-12 precursors were calculated to be 2.02, 1.23, and 1.15 m^2 g^{-1}, respectively.

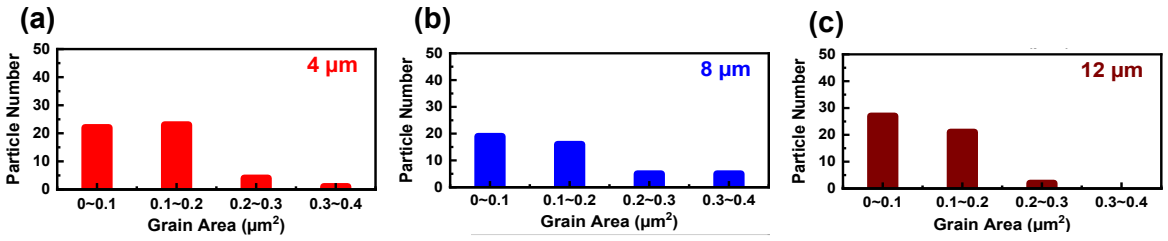

Fig. S2 Grain-area distributions of the selected primary particles, determined via quantitative image analysis: (a) LNO-4, (b) LNO-8, and (c) LNO-12.

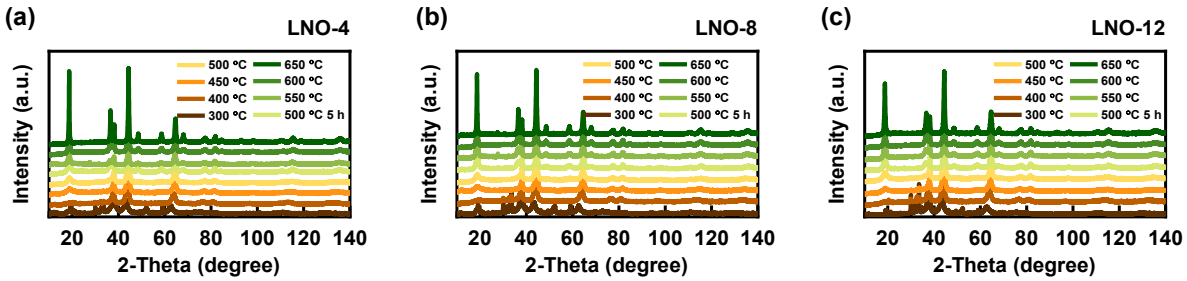

Fig. S3 Ex situ XRD patterns of $LiNiO_2$ synthesized at various calcination temperatures, derived from precursors with varying particle sizes: (a) LNO-4, (b) LNO-8, and (c) LNO-12.

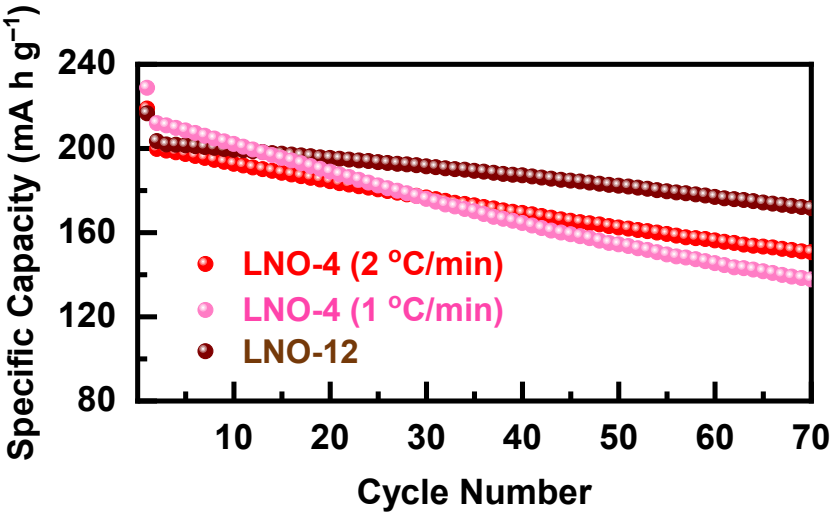

Fig. S4 Cycling performance of LNO-4 synthesized at different heating rates (1 and 2 °C min^{-1}) compared with LNO-12.

Table S1 Crystallographic parameters and Li/Ni site occupancies of the synthesized $LiNiO_2$ samples, extracted via Rietveld refinement of the XRD data

Sample	Lattice Parameter (Å)		*c*/*a* ratio	Grain Size (nm)	$Li_{1-z}Ni_{1+z}O_2$	GOF
	a	*c*				
LNO-4	2.8765	14.1938	4.93	160.4	$Li_{0.934}Ni_{1.066}O_2$	3.40
LNO-8	2.8749	14.1888	4.93	158.2	$Li_{0.988}Ni_{1.012}O_2$	3.25
LNO-12	2.8728	14.1894	4.94	116.3	$Li_{0.993}Ni_{1.007}O_2$	3.38

Table S2 Crystallite size evolution of the $LiNiO_2$ samples synthesized at various calcination temperatures, deduced from ex situ XRD analysis.

Sample	Grain Size (nm)		
	LNO-4	LNO-8	LNO-12
500 ℃ 5 h	9.1	8.6	8.4
550 ℃	10.4	9.4	8.4
600 ℃	19.2	18.5	10.2
650 ℃	22.2	20.5	14.5
650 ℃ 10 h	160.4	158.2	105.1

Table S3 Comparison of the electrochemical performance of representative $LiNiO_2$ cathodes reported in previous studies. The table summarizes the cell configuration, cycling conditions, initial capacity, and capacity retention for half-cell and/or full-cell measurements.

Material	Cell / Condition	Initial Capacity (Half/Full) (mA h g^{-1})	Retention (Half/Full) (%)	Ref
$LiNiO_2$	Half : 4.3 V cutoff / 100 cycles (0.5C) Full : 4.2 V cutoff / 500 cycles (1C/0.5C)	216 / 205	76.7 / 63.4	Our work
$LiNiO_2$	Half : 4.2 V / 100 cycles (0.2C)	190	58	[1]
$LiNiO_2$	Half : 4.3 V / 200 cycles (1C)	183	61	[1]
$LiNiO_2$	Full : 4.2 V / 100 cycles (0.2C)	163	67.6	[1]
$LiNiO_2$	Half : 4.3 V / 100 cycles (0.3C)	207	72	[2]
$LiNiO_2$	Full : 4.2 V / 500 cycles (0.2C)	178	36.5	[3]
$LiNiO_2$	Half : 4.3 V / 50 cycles (0.5C)	157	70	[4]
$LiNiO_2$	Half : 4.3 V / 100 cycles (0.5C)	216	75	[5]
$LiNiO_2$	Half : 4.2 V / 100 cycles (0.5C)	205	76	[6]
$LiNiO_2$	Half : 4.3 V / 100 cycles (1C)	160	51.5	[7]
$LiNiO_2$	Half : 4.3 V / 100 cycles (0.3C)	215	55.8	[8]
$LiNiO_2$	Half : 4.3 V / 100 cycles (0.5C)	196	81.6	[9]
$LiNiO_2$	Full : 4.2 V / 100 cycles (1C)	170	68.4	[10]
$LiNiO_2$	Half : 4.5 V / 100 cycles (0.5C)	160	81.2	[11]
$LiNiO_2$	Half : 4.3 V / 100 cycles (0.1C)	210	76	[12]
$LiNiO_2$	Half : 4.3 V / 100 cycles (0.5C)	230	73.9	[13]

References

[1] R. Narayan, I. Profatilova, R. Dominko and S. Grugeon, *Energy Storage Mater.*, 2025, **79**, 104316.

[2] B. I. J. Johnston, S. Bolloju, S. W. T. Price, S. G. Booth, I. McClelland, L. Ganeshkumar, S. A. Cussen, et al., *J. Mater. Chem. A*, 2025, **13**, 39077–39096.

[3] H. Kaneda, Y. Furuuchi, A. Ikezawa and H. Arai, *ACS Appl. Mater. Interfaces*, 2022, **14**, 52766–52778.

[4] T. T. B. Tran, E.-J. Park, H.-I. Kim, S.-H. Lee, H.-J. Jang and J.-T. Son, *Mater. Lett.*, 2022, **316**, 131810.

[5] W. Shi, L. Liu, R. Xu, R. Sun, J. Dong and X. Kang, *Energy Storage Mater*., 2025, **76**, 104143.

[6] J. Yang, P. Yang, L. Zheng, H. Wang and H. Liu, *ACS Appl. Energy Mater*., 2025, **8**, 7929–7938.

[7] H. Liu, H. Maeda, J. Hwang and K. Matsumoto, *ACS Appl. Mater. Interfaces*, 2024, **16**, 53963–53971.

[8] M. Kim, L. Zou, S.-B. Son, I. D. Bloom, C. Wang and G. Chen, *J. Mater. Chem. A*, 2022, **10**, 12890–12899.

[9] T. T. B. Tran, E.-J. Park, H.-I. Kim, S.-H. Lee, H.-J. Jang and J.-T. Son, *Mater. Lett.*, 2022, **316**, 131810.

[10] R. Narayan, I. Profatilova, R. Dominko and S. Grugeon, *Energy Storage Mater.*, 2025, **79**, 104316.

[11] P. Mohan and G. P. Kalaignan, *Ionics*, 2013, **19**, 895–902.

[12] J. Xu, F. Lin, D. Nordlund, E. J. Crumlin, F. Wang, J. Bai, M. M. Doeff and W. Tong, *Chem. Commun.*, 2016, **52**, 4239–4242.

[13] H.-H. Ryu, G.-T. Park, C. S. Yoon and Y.-K. Sun, *J. Mater. Chem.* A, 2019, **7**, 18580–18588.